

NBSIR 75-659

# A New Mode of Chipping Fracture in Brittle Solids, and Its Application in a Model for Wear Under Fixed Abrasive Conditions

## I. Mode of Chipping Fracture II. Wear Model

---

B. R. Lawn

Inorganic Materials Division  
Institute for Materials Research  
National Bureau of Standards  
Washington, D. C. 20234

February 1975

Interim Report for Period July 1, 1974 through June 30, 1975

Prepared for  
Department of the Navy  
Office of Naval Research  
Arlington, Virginia 22217

Lawn, B. R., Swain, M. V., Phillips, K.,  
On the mode of chipping fracture in brittle  
solids, J. Mater Sci. Lett. 10, 1236-1239  
(1975).

313.

16336

ABSI.R 75-659

Lawn, B. R., A model for the wear of brittle  
solids under fixed abrasive conditions,  
Wear Short Commun. 33, 369-372 (1975).

ABSI.R 75-659  
340

313

16335

**A NEW MODE OF CHIPPING FRACTURE  
IN BRITTLE SOLIDS, AND ITS APPLICATION  
IN A MODEL FOR WEAR UNDER FIXED  
ABRASIVE CONDITIONS**

- I. MODE OF CHIPPING FRACTURE  
II. WEAR MODEL**
- 

B. R. Lawn

Inorganic Materials Division  
Institute for Materials Research  
National Bureau of Standards  
Washington, D. C. 20234

February 1975

Interim Report for Period July 1, 1974 through June 30, 1975

Prepared for  
Department of the Navy  
Office of Naval Research  
Arlington, Virginia 22217



---

**U. S. DEPARTMENT OF COMMERCE, Frederick B. Dent, Secretary  
NATIONAL BUREAU OF STANDARDS, Richard W. Roberts, Director**



## I. On the Mode of Chipping Fracture in Brittle Solids



Chipping processes in brittle solids, despite their unquestionable relevance to a diversity of technologies from ceramics finishing to geological engineering, are not well understood at the fundamental level. Some recent studies of microfracture patterns beneath standard hardness indenters do, however, provide some insight into the problem<sup>1,2</sup>, and it is our objective here to indicate how this insight may be applied to construct a physical model of chipping fracture.

Essentially, the picture which emerges is that depicted in Fig. 1:

- (i) Upon loading the indenter, a confined zone of irreversible (plastic) deformation forms about any sharp points or corners (thereby accounting for the residual hardness impression), from which "median vent" cracks first initiate and subsequently propagate radially outward along suitable planes of symmetry (e.g. as defined by the diagonals of a pyramid indenter, or by preferred cleavage planes) containing the contact axis; (ii) Upon unloading the indenter, the median vents close up, but, just prior to complete removal, "lateral vent" cracks initiate and extend laterally from the deformation zone toward the specimen surface. Of the two types of cracking it is clearly the second which relates more directly to brittle chipping.

Yet up till now a detailed fracture mechanics analysis has been attempted only for the median vent system. This system is relatively well defined, since the indentation stress field, which uniquely determines the extent of crack growth<sup>1</sup>, can reasonably be represented in terms of the classical Boussinesq field for normal point loading<sup>2, 3</sup>. On the basis of the fundamental Griffith energy-balance condition for fracture<sup>4</sup>, it may readily be argued that brittle cracks will generally

tend to follow trajectories of the lesser principal stresses within the indentation field, such that the path maintains near-orthogonality to a component of major tension: the best studied illustration of this principle is the Hertzian cone crack<sup>5, 6</sup>, which, in the absence of any deformation-induced nucleation center, initiates from an incipient surface flaw and flares downward into the specimen.

In the scheme of Fig. 2, in which the principal stresses are defined such that  $\sigma_{11} > \sigma_{22} > \sigma_{33}$  (positive values denoting tension) nearly everywhere, median vent geometry may be specified in terms of families of  $\sigma_{11}$  and  $\sigma_{33}$  trajectories, cone crack geometry in terms of families of  $\sigma_{22}$  and  $\sigma_{33}$  trajectories.

The conditions under which the lateral vents form are, unfortunately, less easily modelled. Since the lateral system operates only as the indenter is withdrawn from the specimen surface it is evident that the driving force for propagation must originate from some residual stress field associated with the irreversible deformation zone.

This conclusion is substantiated by microscopic investigation of the damage patterns as a function of indenter geometry (e.g. "sharp" or "blunt"): in general, the extent of lateral venting is found to increase markedly with expanding zone size. A graphic illustration of the effect is obtained by loading a soda-lime glass plate with a small (1mm diam.) spherical indenter: at comparatively low load the contact is elastic, and the only fracture is that of cone cracking, whereas at higher load some plasticity develops beneath the penetrating sphere, and lateral venting becomes evident in the unloaded plate.<sup>1</sup> A related effect was reported by Culf<sup>7</sup>, who observed otherwise

regular cone cracks in glass to deflect upward ("hat brim" effect) upon sudden release of the indenter load. Culf also observed considerable residual stress birefringence in association with this phenomenon, over distances large compared with the scale of the deformation zone itself. That residual stresses exist about hardness impressions in most brittle materials has been amply demonstrated by a number of strain-sensitive techniques<sup>8</sup>. That these stresses can also be moderately long-range in nature is seen most clearly in the distances over which relaxation by plastic flow (e.g. dislocation loop punching) occurs in annealing experiments<sup>9</sup>. Neither the existence nor the intensity of the residual elastic fields should come as any surprise, for the stress levels achieved beneath the indenter in hardness tests on highly brittle solids tend to be of the order of the intrinsic bond strength of the structure<sup>10, 11</sup>, and the relief of these high stresses would ideally require the impressed region to restore completely to its original unstrained state.

These observations, coupled with a reexamination of the Boussinesq field, provide us with a working model upon which to base an analysis of lateral vent formation. We note that the lateral vents extend in all cases on surfaces closely delineated by families of  $\sigma_{11}$  and  $\sigma_{22}$  trajectories in Fig. 2 (although the paths are modified somewhat by the deformation zone itself, and by free surfaces, including any preexisting median vents or cone cracks); it is as if the applied load were actually reversed upon indenter withdrawal, so that the  $\sigma_{33}$  stress normal to the lateral vent becomes the dominant component of tension in the field. Of course, it is

physically meaningless to associate a reversed applied load with a surface in the unloaded state, but an effectively similar net result may obtain if the deformation zone were to act as a center of contraction with respect to the surrounding elastic matrix. This effect is depicted schematically in Fig. 3. The distribution of stresses at the zone boundary must inevitably depend strongly on the nature of the irreversible deformation (which itself remains an issue of some controversy<sup>11, 12</sup>). Nevertheless, one can proceed by making reasonable assumptions as to this distribution (e.g. that the tractions are of constant magnitude, and are directed such that the net force is zero), and evaluate the residual field in the matrix by taking expressions for the stresses due to elemental point forces (e.g. Mindlin<sup>13</sup>) and integrating around the boundary. One may then construct a stress trajectory pattern for the field, in analogy to Fig. 2, and thereby trace out prospective fracture paths from the deformation zone. Full details of such calculations will be discussed elsewhere; we simply report here that the predicted paths do indeed curve toward the specimen surface in essentially the manner shown in Fig. 1.

The scope of the present model extends well beyond the establishment of a suitable basis for evaluating an "index of brittleness" in standard hardness testing<sup>14</sup>. It provides physical insight into a number of seemingly unrelated phenomena in brittle solids:

- (i) Strength degradation. Surface damage introduced into a brittle surface as a result of contact (either static or impact) with hard particles constitutes a potential source of weakness. The mechanics of the damage process may be conveniently simulated in a simple indentation test<sup>15</sup>.

(ii) Glass cutting. A glass cutter's wheel is designed to produce a continuous "trailing" median vent as a linear starting crack for subsequent plate fracture in flexure. However, lateral venting invariably occurs in the wake of the moving "indenter", thereby damaging the edges of the final cut. Clearly, the need here is for a means of suppressing the chipping mode.

(iii) Surface removal processes. Individual chipping events in the machining, drilling, grinding, abrasion, erosion and wear of brittle surfaces in general (e.g. ceramics, gemstones, rocks) are of the type depicted in Fig. 1<sup>1</sup>. By summing over an appropriate distribution of such microscopic events, it should be possible to describe macroscopic surface removal parameters at a fundamental level.

(iv) Geophysical impact phenomena. Meteorite-induced craters ranging in scale from geological land masses<sup>16</sup> to lunar fines<sup>17</sup> bear a resemblance to the damage pattern in Fig. 1 which can only be described as striking. While thermal and stress-wave effects associated with the high-velocity impacts are undoubtedly important factors in these cases<sup>18</sup>, the possible role of residual stresses about the central "deformation zone" in determining crater morphology may warrant further attention.

B. R. Lawn

Institute for Materials Research  
National Bureau of Standards  
Washington, D. C. 20234  
U. S. A.

M. V. Swain

Martin Marietta Laboratories  
1450 South Rolling Road  
Baltimore, Md. 21227  
U. S. A.

K. Phillips

Division of Materials Science  
University of Sussex  
Falmer, Sussex BN1 9QT  
England

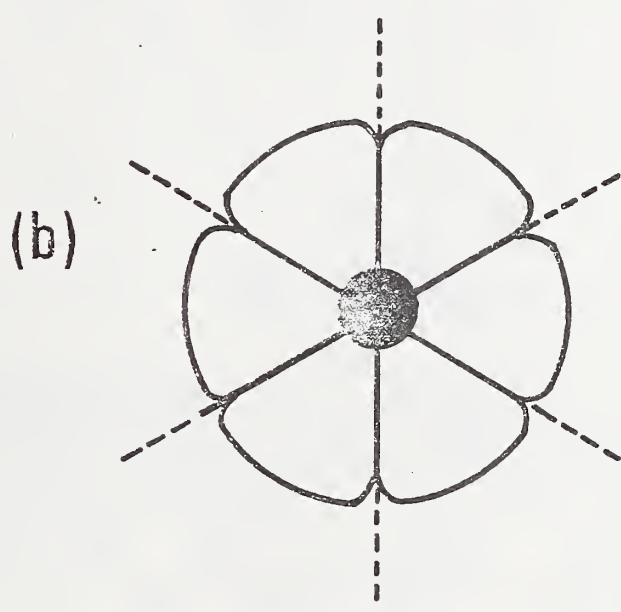
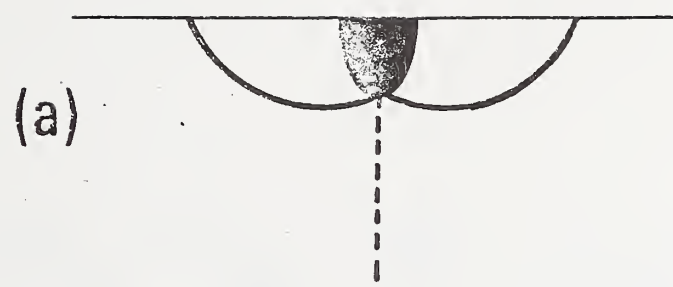
## References

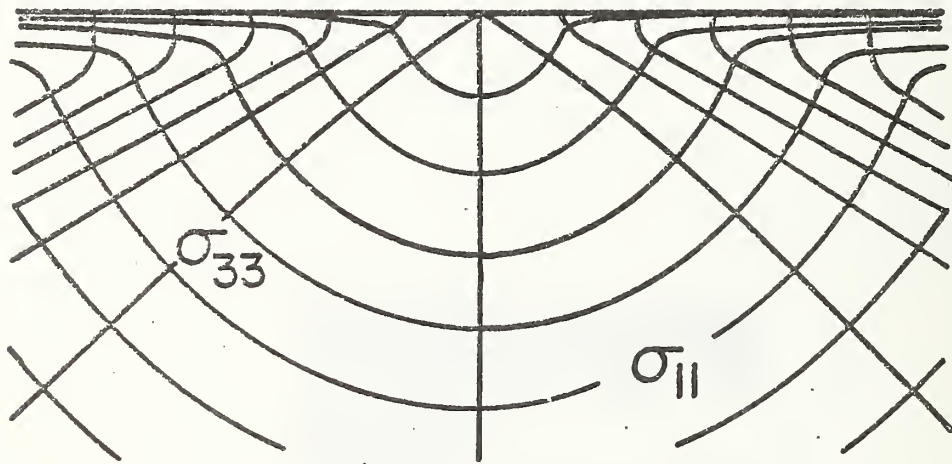
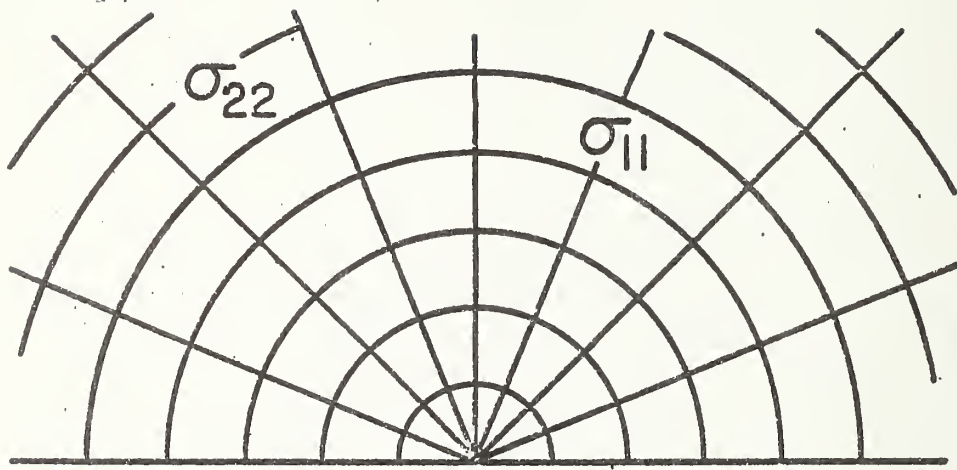
1. Lawn, B. R. and Wilshaw, T. R., J. Mater. Sci., in the press.
2. Lawn, B. R. and Swain, M. V., J. Mater. Sci., in the press.
3. Boussinesq, J., Application des Potentiels a l'Etude de l'Equilibre et du Mouvement des Solides Elastiques, (Gauthier-Villars, Paris, 1885). Discussed in Timoshenko, S. P. and Goodier, J. N., Theory of Elasticity (McGraw-Hill, New York, 1970), pp. 398-402.
4. Griffith, A. A., Phil. Trans. Roy. Soc. Lond., A211, 163 (1920).
5. Hertz, H., J. Reine Angew. Math., 92, 156 (1881); Verhandlungen des Vereins zur Beforderung des Gewerbe Fleisses, 61, 449 (1882). Reprinted in English, in Hertz's Miscellaneous Papers (Macmillian, London, 1896), Chs. 5, 6.
6. Frank, F. C. and Lawn, B. R., Proc. Roy. Soc. Lond., A299, 291 (1967).
7. Culf, C. J., J. Soc. Glass.Tech., 41, 157 (1957).
8. Hockey, B. J., in The Science of Hardness Testing and its Research Applications, Symposium Proceedings, Eds. Westbrook, J. H. and Conrad, H. (American Society for Metals, Metals Park, 1973), Ch. 3.
9. Wagatsume, R., Sumino, K., Uchida, W. and Yamamoto, S. J. Appl. Phys., 42, 222 (1971).
10. Kelly, A., Strong Solids (Clarendon, Oxford, 1966).
11. Hill, M. J. and Rowcliffe, D. J., J. Mater. Sci., in the press.
12. Ernsberger, F. M., Ann. Rev. Mat. Sci., 2, 529 (1972).
13. Mindlin, R. D., Physics, 7, 195 (1936).
14. Westbrook, J. H., in The Science of Hardness Testing and its Research Applications, Symposium Proceedings, Eds. Westbrook, J. H. and Conrad, H. (American Society for Metals, Metals Park, 1973), pp. 491-494.

15. Evans, A. G., J. Amer. Ceram. Soc., 56, 405 (1973).
16. Nadai, A., Theory of Flow and Fracture of Solids (McGraw-Hill, New York, 1963), pp. 247-249.
17. Carter, J. L. and MacGregor, I. D., Proc. Apollo 11 Lunar Sci. Conf., 1, 247 (1970).
18. Vedder, J. F. and Mandeville, J.-C., J. Geophys. Res., 79, 3247 (1974).

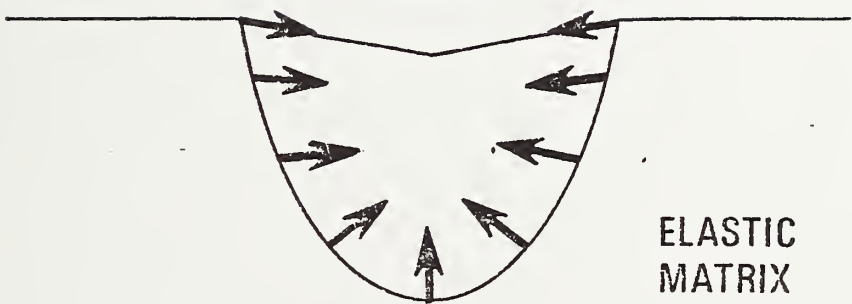
### Figure Captions

1. Fracture geometry beneath sharp indenter. Central deformation zone shown as dark region, median vent cracks as broken lines, lateral vent cracks as heavy lines. (a) Section view schematic, (b) plan view schematic, (c) surface view of fused silica indented with sharp, irregular particle (scanning electron micrograph, field width 3mm).
2. Stress trajectories (curves whose tangent indicates direction of principal stress) for Boussinesq field, showing half-surface view (top) and section view (bottom). Cone cracks initiate from incipient surface flaws and propagate everywhere orthogonally to  $\sigma_{11}$  (tensile outside contact area), median vents initiate from central deformation zone and propagate orthogonally to  $\sigma_{22}$  (tensile below contact zone), lateral vents initiate from deformation zone and propagate nearly orthogonally to  $\sigma_{33}$  (compressive everywhere, but tensile if applied load reversed).
3. Schematic representation of distribution of mismatch tractions at boundary between central deformation zone and surrounding elastic matrix, at indenter withdrawal.





**DEFORMATION  
ZONE**





II. A Model for the Wear of Brittle Solids  
Under Fixed Abrasive Conditions



Other than that the wear mechanism involves some microfracturing, and the wear rate is remarkably high, relatively little is known about the abrasion of highly brittle solids<sup>1,2</sup>; this despite intense current interest in the machining and finishing of brittle surfaces within the ceramics engineering industry<sup>3</sup>. However, with the advent of "indentation fracture mechanics" a new approach has become available for investigating a wide range of small-scale cracking phenomena<sup>4</sup>. The purpose of the present note is to use this approach to construct an explicit model of the wear process in brittle solids, for the simple case of a "fixed" abrasive medium ("two-body" process) in which the grit particles are "ideally sharp."

A schematic representation of the wear mechanism is given in Figure 1. Macroscopically, one measures the wear rate  $\dot{V} = dV/dt$  ( $V$  = volume removed) appropriate to a specified total load  $P$  and velocity  $v_0$  for the abrasive medium relative to the specimen. Microscopically, attention focusses on the individual chip-removal mechanism, characterized by an "indenter" load  $P_i$  and velocity  $v_{i0}$  (all "indenters" traverse the specimen with the same velocity in the two-body configuration). The idea is to start with a mechanical description of the removal process for the  $i$  th indenter, and thence to sum over all such  $i$  events to predict the macroscopic behavior.

To this end we resort to observations in "model" brittle solids (notably glass) of the fracture patterns beneath standard sharp indenters (e.g. cones, pyramids)<sup>5,6</sup>, to build up the following picture. We consider the sliding particle  $i$  to produce a "plastic"

deformation track of width  $2\bar{a}_i$ . Then, for geometrically similar impressions, the mean indentation pressure at any instant of contact may be identified with the material hardness<sup>7</sup>,

$$\underline{p}_i = \underline{P}_i / \alpha \pi \bar{a}_i^2 \approx H, \quad (1)$$

where  $\alpha$  is a factor determined by indenter geometry. Upon unloading, residual stresses, associated with incompatibility between deformation zone and surrounding elastic matrix, initiate and propagate lateral, chip-forming cracks (so-called "lateral vents"; other cracks form on loading, but these extend straight downward, and play only a secondary role in chipping). In this view, the size of the prospective chip is determined by the configuration of the hardness impression, so the chip area may be written

$$\underline{A}_i = \eta \bar{a}_i^2, \quad (2)$$

where  $\eta$  is a linear scaling factor. The volume of material removed by the indenting particle in traversing through a distance  $\Delta \underline{l}$  in an interval of time  $\Delta \underline{t}$  is  $\Delta \underline{V}_i = \underline{A}_i \Delta \underline{l}$ , whence, from (1) and (2),

$$\dot{\underline{V}}_i = \Delta \underline{V}_i / \Delta \underline{t} = \underline{A}_i \Delta \underline{l} / \Delta \underline{t} = (\eta v_o / \alpha \pi H) \underline{P}_i. \quad (3)$$

A straightforward summation operation now gives the macroscopic wear rate;

$$\dot{V} = \sum_{i=1}^N \dot{v}_i = (\eta v_o / \alpha \pi H) \sum_{i=1}^N p_i = \eta v_o P / \alpha \pi H. \quad (4)$$

This equation may be rearranged,

$$\dot{V} / v_o P = \eta / \alpha \pi H, \quad (5)$$

such that the left and right sides conveniently represent macroscopic and microscopic parameters respectively.\* It would thus appear possible to predetermine the abrasive wear rate of brittle ceramics simply from quantities measured in standard hardness testing procedures.

Some data from soda-lime glass illustrate the principle. Taking  $H \approx 1.0 \times 10^{10} \text{ Nm}^{-2}$  ("dynamic" hardness)<sup>8</sup>,  $\alpha \approx 1$  (conical particles),  $\eta \approx 1$ , we predict  $\eta / \alpha \pi H \approx 3 \times 10^{-11} \text{ m}^2 \text{ N}^{-1}$  as the wear rate. This compares with  $\dot{V} / v_o P \approx 1 \times 10^{-11} \text{ m}^2 \text{ N}^{-1}$  measured under test conditions in which chipping is pronounced (namely, spherical specimens on an alumina grinding block pre-ground with 45μm diamond paste, decyl alcohol environment, at  $P = 10 \text{ N}$ ,  $v_o = 1 \text{ ms}^{-1}$ )<sup>9</sup>.

There are some interesting implications associated with the present model:

(i) The calculated wear rate is independent of the (apparent) area of contact between work tool and specimen, and also of the number and size of indenting particles. Thus, all arbitrariness and complication of a statistical analysis is avoided. Physically, this

\*A term equivalent to that on the left of (5),  $\Delta V / P \Delta l$ , is often used as an alternative expression of the macroscopic wear rate.

arises because of the essential "linearity" of the fixed-abrasive wear mechanism: the chip volume is proportional to the load on the indenting particle, so that the total volume removed does not depend on the way in which the total load is distributed.

(ii) The analysis tacitly assumes that the intensity of the residual stress field about the deformation track is sufficiently high to drive the chip-forming cracks to the surface. The indication from indentation fracture mechanics studies<sup>10</sup> is that the extent of micro-cracking relative to the size of the deformation zone diminishes with decreasing load. Thus we might anticipate a brittle-to-ductile, chipping-to-ploughing transition in wear mechanism at low abrasion loads, small particle sizes, with an attendant fall in wear rate to a value more typical of non-brittle solids<sup>1</sup>. Again, it has been assumed that geometrical similarity is preserved in the indentation fracture process. In practice, initially sharp particles tend to become "blunt" (either by fragmentation or by clogging with debris), and intersections tend to occur between neighboring tracks, as abrasion proceeds; these effects will further reduce the wear rate.

(iii) Most significantly, the wear rate under ideal chipping conditions is uniquely determined by the material hardness; by controlling the scale of the crack pattern behind the indenting particle, the "plasticity" properties of the material assume a key role in the abrasion process. However, hardness is a rate-dependent quantity which can change markedly with the conditions of testing, e.g. environment, load rate (sliding velocity), etc.<sup>8,11</sup> This bears strongly on the

correlations between a wide range of chemo-mechanical properties (e.g. machining, drilling, grinding) and the hardness of brittle materials reported by Westwood and co-workers<sup>12</sup>. While the present model may provide a sound basis for interpreting chemo-mechanical phenomena, it needs to be emphasised that correlations of this type can be truly meaningful only if the hardness values are measured under conditions pertinent to the macroscopic situation.

Acknowledgements

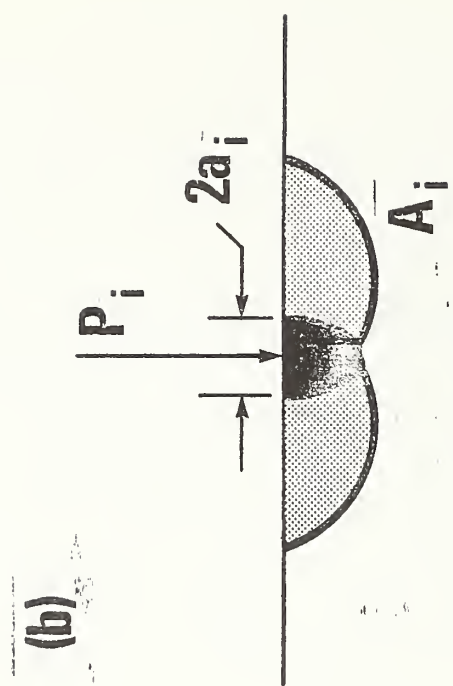
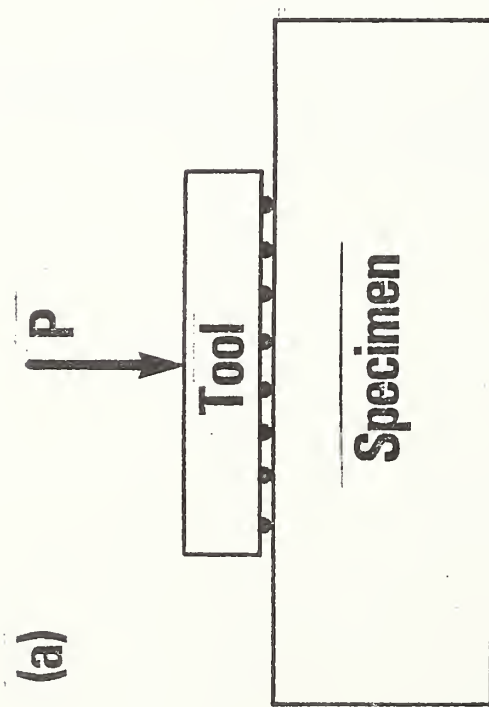
The author is indebted to S. M. Wiederhorn and H. H. Johnson for discussions on this work. The sponsorship by the Office of Naval Research, under Contract No. NR-032-535, is acknowledged.

Figure Captions

1. Cross-sectional views of "fixed" abrasion process. (a) Macroscopic view: total load  $\underline{P}$  bears on specimen via abrasive grit particles bonded to tool. (b) Microscopic view:  $i$  th particle experiences load  $\underline{P}_i$ , and leaves in its wake a deformation track, width  $2\underline{a}_i$ , from which "lateral vents" propagate to form chip, section area  $\underline{A}_i$ . All particles translate across specimen surface with velocity  $\underline{v}_o$ .

## References

1. E. Rabinowicz, Friction and Wear of Materials, Wiley, New York, 1965, Ch. 7.
2. M. M. Krushev, Wear, 28 (1974) 69.
3. The Science of Ceramic Machining and Surface Finishing, Symposium Proceedings, N. B. S. Special Publ. 348, 1972.
4. B. R. Lawn and T. R. Wilshaw, J. Mater. Sci. (in press).
5. B. R. Lawn and M. V. Swain, J. Mater. Sci. (in press).
6. B. R. Lawn, M. V. Swain and K. Phillips, to be published.
7. D. Tabor, The Hardness of Metals, Clarendon, Oxford, 1951, Ch. 1.
8. S. P. Gunasekera and D. G. Holloway, Phys. and Chem. Glasses, 14 (1973) 45.
9. S. M. Wiederhorn and D. E. Roberts, Wear, 32 (1975) 51.
10. B. R. Lawn and E. R. Fuller, to be published.
11. R. E. Hanneman and J. H. Westbrook, Phil. Mag. 18 (1968) 73.
12. A. R. C. Westwood and N. H. Macmillan, The Science of Hardness Testing and its Research Applications, Symposium Proceedings, American Society for Metals, 1973, Ch. 28.



A MODEL FOR THE WEAR OF BRITTLE SOLIDS

---

UNDER FIXED ABRASIVE CONDITIONS

B. R. Lawn\*

Institute for Materials Research, National Bureau of Standards,  
Washington, D. C. 20234, U.S.A.

---

\*On study leave, from School of Physics, University of New South Wales,  
Kensington, N. S. W. 2033, Australia



Other than that the wear mechanism involves some microfracturing, and the wear rate is remarkably high, relatively little is known about the abrasion of highly brittle solids<sup>1,2</sup>; this despite intense current interest in the machining and finishing of brittle surfaces within the ceramics engineering industry<sup>3</sup>. However, with the advent of "indentation fracture mechanics" a new approach has become available for investigating a wide range of small-scale cracking phenomena<sup>4</sup>. The purpose of the present note is to use this approach to construct an explicit model of the wear process in brittle solids, for the simple case of a "fixed" abrasive medium ("two-body" process) in which the grit particles are "ideally sharp."

A schematic representation of the wear mechanism is given in Figure 1. Macroscopically, one measures the wear rate  $\dot{V} = dV/dt$  ( $V$  = volume removed) appropriate to a specified total load  $P$  and velocity  $v_0$  for the abrasive medium relative to the specimen. Microscopically, attention focusses on the individual chip-removal mechanism, characterized by an "indenter" load  $P_i$  and velocity  $v_0$  (all "indenters" traverse the specimen with the same velocity in the two-body configuration). The idea is to start with a mechanical description of the removal process for the  $i$  th indenter, and thence to sum over all such  $i$  events to predict the macroscopic behavior.

To this end we resort to observations in "model" brittle solids (notably glass) of the fracture patterns beneath standard sharp indenters (e.g. cones, pyramids)<sup>5,6</sup>, to build up the following picture. We consider the sliding particle  $i$  to produce a "plastic"

deformation track of width  $2\bar{a}_i$ . Then, for geometrically similar impressions, the mean indentation pressure at any instant of contact may be identified with the material hardness<sup>7</sup>,

$$\underline{p}_i = \underline{p}_i / \alpha \pi \bar{a}_i^2 \approx \underline{H}, \quad (1)$$

where  $\alpha$  is a factor determined by indenter geometry. Upon unloading, residual stresses, associated with incompatibility between deformation zone and surrounding elastic matrix, initiate and propagate lateral, chip-forming cracks (so-called "lateral vents"; other cracks form on loading, but these extend straight downward, and play only a secondary role in chipping). In this view, the size of the prospective chip is determined by the configuration of the hardness impression, so the chip area may be written

$$\underline{A}_i = \underline{n} \bar{a}_i^2, \quad (2)$$

where  $\underline{n}$  is a linear scaling factor. The volume of material removed by the indenting particle in traversing through a distance  $\Delta \underline{l}$  in an interval of time  $\Delta \underline{t}$  is  $\Delta \underline{V}_i = \underline{A}_i \Delta \underline{l}$ , whence, from (1) and (2),

$$\dot{\underline{V}}_i = \Delta \underline{V}_i / \Delta \underline{t} = \underline{A}_i \Delta \underline{l} / \Delta \underline{t} = (\underline{n} \underline{v}_o / \alpha \pi \underline{H}) \underline{p}_i. \quad (3)$$

A straightforward summation operation now gives the macroscopic wear rate;

$$\dot{V} = \sum_{i=1}^N \dot{v}_i = (\eta v_o / \alpha \pi H) \sum_{i=1}^N p_i = \eta v_o P / \alpha \pi H. \quad (4)$$

This equation may be rearranged,

$$\dot{V} / v_o P = \eta / \alpha \pi H, \quad (5)$$

such that the left and right sides conveniently represent macroscopic and microscopic parameters respectively.\* It would thus appear possible to predetermine the abrasive wear rate of brittle ceramics simply from quantities measured in standard hardness testing procedures.

Some data from soda-lime glass illustrate the principle. Taking  $H \approx 1.0 \times 10^{10} \text{ Nm}^{-2}$  ("dynamic" hardness)<sup>8</sup>,  $\alpha \approx 1$  (conical particles),  $\eta \approx 1$ , we predict  $\eta / \alpha \pi H \approx 3 \times 10^{-11} \text{ m}^2 \text{ N}^{-1}$  as the wear rate. This compares with  $\dot{V} / v_o P \approx 1 \times 10^{-11} \text{ m}^2 \text{ N}^{-1}$  measured under test conditions in which chipping is pronounced (namely, spherical specimens on an alumina grinding block pre-ground with 45µm diamond paste, decyl alcohol environment, at  $P = 10 \text{ N}$ ,  $v_o = 1 \text{ ms}^{-1}$ )<sup>9</sup>.

There are some interesting implications associated with the present model:

(i) The calculated wear rate is independent of the (apparent) area of contact between work tool and specimen, and also of the number and size of indenting particles. Thus, all arbitrariness and complication of a statistical analysis is avoided. Physically, this

\*A term equivalent to that on the left of (5),  $\Delta V / P \Delta t$ , is often used as an alternative expression of the macroscopic wear rate.

arises because of the essential "linearity" of the fixed-abrasive wear mechanism: the chip volume is proportional to the load on the indenting particle, so that the total volume removed does not depend on the way in which the total load is distributed.

(ii) The analysis tacitly assumes that the intensity of the residual stress field about the deformation track is sufficiently high to drive the chip-forming cracks to the surface. The indication from indentation fracture mechanics studies<sup>10</sup> is that the extent of micro-cracking relative to the size of the deformation zone diminishes with decreasing load. Thus we might anticipate a brittle-to-ductile, chipping-to-ploughing transition in wear mechanism at low abrasion loads, small particle sizes, with an attendant fall in wear rate to a value more typical of non-brittle solids<sup>1</sup>. Again, it has been assumed that geometrical similarity is preserved in the indentation fracture process. In practice, initially sharp particles tend to become "blunt" (either by fragmentation or by clogging with debris), and intersections tend to occur between neighboring tracks, as abrasion proceeds; these effects will further reduce the wear rate.

(iii) Most significantly, the wear rate under ideal chipping conditions is uniquely determined by the material hardness; by controlling the scale of the crack pattern behind the indenting particle, the "plasticity" properties of the material assume a key role in the abrasion process. However, hardness is a rate-dependent quantity which can change markedly with the conditions of testing, e.g. environment, load rate (sliding velocity), etc.<sup>8,11</sup> This bears strongly on the

correlations between a wide range of chemo-mechanical properties (e.g. machining, drilling, grinding) and the hardness of brittle materials reported by Westwood and co-workers<sup>12</sup>. While the present model may provide a sound basis for interpreting chemo-mechanical phenomena, it needs to be emphasised that correlations of this type can be truly meaningful only if the hardness values are measured under conditions pertinent to the macroscopic situation.

Acknowledgements

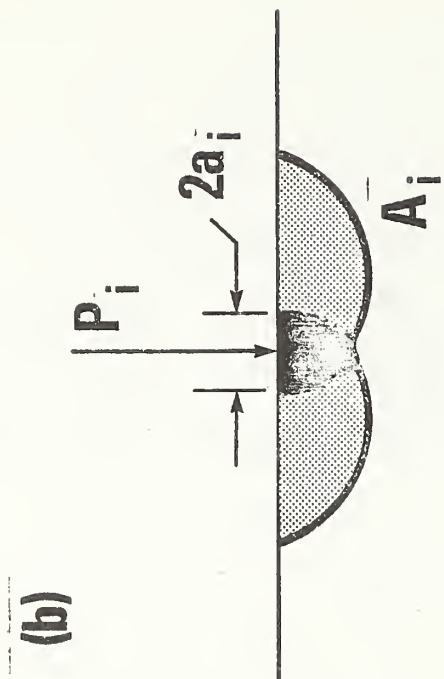
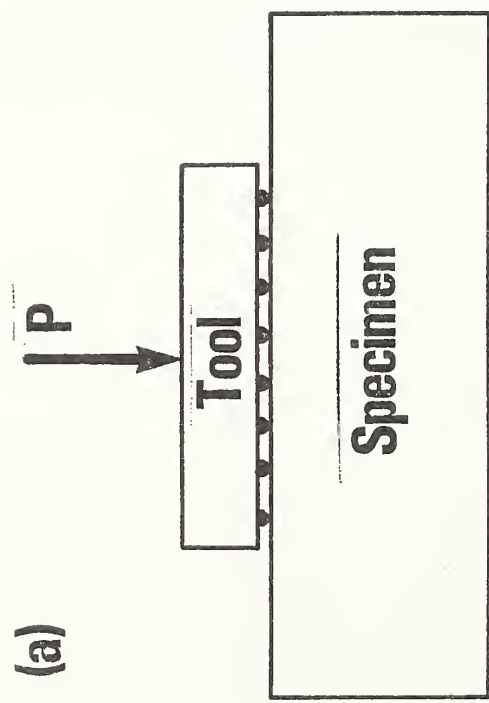
The author is indebted to S. M. Wiederhorn and H. H. Johnson for discussions on this work. The sponsorship by the Office of Naval Research, under Contract No. NR-032-535, is acknowledged.

## References

1. E. Rabinowicz, Friction and Wear of Materials, Wiley, New York, 1965, Ch. 7.
2. M. M. Krushev, Wear, 28 (1974) 69.
3. The Science of Ceramic Machining and Surface Finishing, Symposium Proceedings, N. B. S. Special Publ. 348, 1972.
4. B. R. Lawn and T. R. Wilshaw, J. Mater. Sci. (in press).
5. B. R. Lawn and M. V. Swain, J. Mater. Sci. (in press).
6. B. R. Lawn, M. V. Swain and K. Phillips, to be published.
7. D. Tabor, The Hardness of Metals, Clarendon, Oxford, 1951, Ch. 1.
8. S. P. Gunasekera and D. G. Holloway, Phys. and Chem. Glasses, 14 (1973) 45.
9. S. M. Wiederhorn and D. E. Roberts, Wear, 32 (1975) 51.
10. B. R. Lawn and E. R. Fuller, to be published.
11. R. E. Hanneman and J. H. Westbrook, Phil. Mag. 18 (1968) 73.
12. A. R. C. Westwood and N. H. Macmillan, The Science of Hardness Testing and its Research Applications, Symposium Proceedings, American Society for Metals, 1973, Ch. 28.

Figure Captions

1. Cross-sectional views of "fixed" abrasion process. (a) Macroscopic view: total load  $\underline{P}$  bears on specimen via abrasive grit particles bonded to tool. (b) Microscopic view:  $i$  th particle experiences load  $\underline{P}_i$ , and leaves in its wake a deformation track, width  $2\underline{a}_i$ , from which "lateral vents" propagate to form chip, section area  $\underline{A}_i$ . All particles translate across specimen surface with velocity  $\underline{v}_o$ .



## On the Mode of Chipping Fracture in Brittle Solids

Chipping processes in brittle solids, despite their unquestionable relevance to a diversity of technologies from ceramics finishing to geological engineering, are not well understood at the fundamental level. Some recent studies of microfracture patterns beneath standard hardness indenters do, however, shed some light on the problem<sup>1, 2</sup>.

Essentially, the picture which emerges is that depicted in Fig. 1:

(i) Upon loading the indenter a confined zone of irreversible (plastic) deformation forms about any sharp points or corners (thereby accounting for the residual hardness impression), from which "median vent" cracks first initiate and subsequently propagate radially outward along suitable planes of symmetry (e.g. as defined by the diagonals of a pyramid indenter, or by preferred cleavage planes) containing the contact axis; (ii) Upon unloading the indenter the median vents close up, but, just prior to complete removal, "lateral vent" cracks initiate and extend laterally from the deformation zone toward the specimen surface. Of the two types of cracking it is clearly the second which relates more directly to brittle chipping.

Yet up till now a detailed fracture mechanics analysis has been attempted only for the median vent system. This system is relatively well defined, since the indentation stress field, which uniquely determines the extent of crack growth<sup>1</sup>, can reasonably be represented in terms of the classical Boussinesq field for normal point loading<sup>2, 3</sup>. On the basis of the fundamental Griffith energy-balance condition for fracture<sup>4</sup> it may readily be argued that brittle cracks will generally

tend to follow trajectories of the lesser principal stresses within the indentation field, such that the path maintains near-orthogonality to a component of major tension: the best-studied illustration of this principle is the Hertzian cone crack<sup>5, 6</sup>, which, in the absence of any deformation-induced nucleation center, initiates from an incipient surface flaw and flares downward into the specimen.

In the scheme of Fig. 2, in which the principal stresses are defined such that  $\sigma_{11} > \sigma_{22} > \sigma_{33}$  (positive values denoting tension) nearly everywhere, median vent geometry may be specified in terms of families of  $\sigma_{11}$  and  $\sigma_{33}$  trajectories, cone crack geometry in terms of families of  $\sigma_{22}$  and  $\sigma_{33}$  trajectories.

The conditions under which the lateral vents form are, unfortunately, less easily modelled. Since the lateral system operates only as the indenter is withdrawn from the specimen surface it is evident that the driving force for propagation must originate from some residual stress field associated with the irreversible deformation zone.

This conclusion is substantiated by microscopic investigation of the damage patterns as a function of indenter geometry (e.g. "sharp" or "blunt"): in general, the extent of lateral venting is found to increase markedly with expanding zone size. A graphic illustration of the effect is obtained by loading a soda-lime glass plate with a small (1mm diam.) spherical indenter: at comparatively low load the contact is elastic, and the only fracture is that of cone cracking, whereas at higher load some plasticity develops beneath the penetrating sphere, and lateral venting begins to establish itself<sup>1</sup>. A manifestation of this behavior was reported by Culf<sup>7</sup>, who observed otherwise

regular cone cracks in glass to deflect upward ("hat brim" effect) upon sudden release of the indenter load. Culf also observed considerable residual stress birefringence in association with this phenomenon, over distances large compared with the scale of the deformation zone itself. That residual stresses exist about hardness impressions in most brittle materials has been amply demonstrated by a number of strain-sensitive techniques<sup>8</sup>. That these stresses can also be moderately long-range in nature is seen most clearly in the distances over which relaxation by plastic flow (e.g. dislocation loop punching) occurs in annealing experiments<sup>9</sup>. Neither the existence nor the intensity of the residual elastic fields should come as any surprise, for the stress levels achieved beneath the indenter in hardness tests on highly brittle solids tend to be of the order of the intrinsic bond strength of the structure<sup>10, 11</sup>, and the relief of these high stresses would ideally require the impressed region to restore completely to its original unstrained state.

These observations, coupled with a reexamination of the Boussinesq field, provide us with the basis for an analysis of lateral vent geometry. We note that the lateral vents extend in all cases on surfaces closely delineated by families of  $\sigma_{11}$  and  $\sigma_{22}$  trajectories in Fig. 2 (although the paths are modified somewhat by the deformation zone itself, and by free surfaces, including any preexisting median vents or cone cracks); it is as if the applied load were actually reversed upon indenter withdrawal, so that the  $\sigma_{33}$  stress normal to the lateral vent becomes the dominant component of tension in the field. Of course, it is

physically meaningless to associate a reversed applied load with a surface in the unloaded state, but an effectively similar net result may obtain if the deformation zone were to act as a center of contraction with respect to the surrounding elastic matrix. This is depicted schematically in Fig. 3. The distribution of stresses at the zone boundary must inevitably depend strongly on the nature of the irreversible deformation, which itself remains an issue of some controversy<sup>11, 12</sup>.

Nevertheless, one can proceed by making reasonable assumptions as to this distribution (e.g. that the tractions are of constant magnitude, and are directed such that the net force is zero), and evaluate the residual field in the matrix by taking expressions for the stresses due to elemental point forces (e.g. Mindlin<sup>13</sup>) and integrating around the boundary. One may then construct a stress trajectory pattern for the field, in analogy to Fig. 2, and thereby trace out probable fracture paths from the deformation zone. Full details of such calculations will be discussed elsewhere; we simply report here that the predicted paths do indeed curve toward the specimen surface in essentially the manner shown in Fig. 1.

The scope of the present model extends well beyond the establishment of a suitable basis for evaluating an "index of brittleness" in standard hardness testing<sup>14</sup>. It provides physical insight into a number of seemingly unrelated phenomena in brittle solids:

(i) Strength degradation. Surface damage introduced into a brittle surface as a result of contact (either static or impact) with hard particles constitutes a potential source of weakness. The mechanics of the damage process may be conveniently simulated in a simple indentation test<sup>15</sup>.

(ii) Glass cutting. A glass cutter's wheel is designed to produce a continuous "trailing" median vent as a linear starting crack for subsequent plate fracture in flexure. However, lateral venting invariably occurs in the wake of the moving "indenter", thereby damaging the edges of the final cut. Clearly, the objective here is to find a way of suppressing the chipping mode.

(iii) Surface removal processes. Individual chipping events in the machining, drilling, grinding, abrasion, erosion and wear of brittle surfaces in general (e.g. ceramics, gemstones, rocks) are of the type depicted in Fig. 1<sup>1</sup>. By summing over an appropriate distribution of such microscopic events it should be possible to describe macroscopic surface removal parameters at a fundamental level.

(iv) Geophysical impact phenomena. Meteorite-induced craters ranging in scale from geological land masses<sup>16</sup> to lunar fines<sup>17</sup> bear a resemblance to the damage pattern in Fig. 1 which can only be described as striking. While thermal and stress-wave effects associated with the high-velocity impacts are undoubtedly important factors in these cases<sup>18</sup>, the possible role of residual stresses about the central "deformation zone" in determining crater morphology may warrant further attention.

B. R. Lawn

Institute for Materials Research  
National Bureau of Standards  
Washington, D. C. 20234  
U. S. A.

M. V. Swain

Martin Marietta Laboratories  
1450 South Rolling Road  
Baltimore, Md. 21227  
U. S. A.

K. Phillips

Division of Materials Science  
University of Sussex  
Falmer, Sussex BN1 9QT  
England

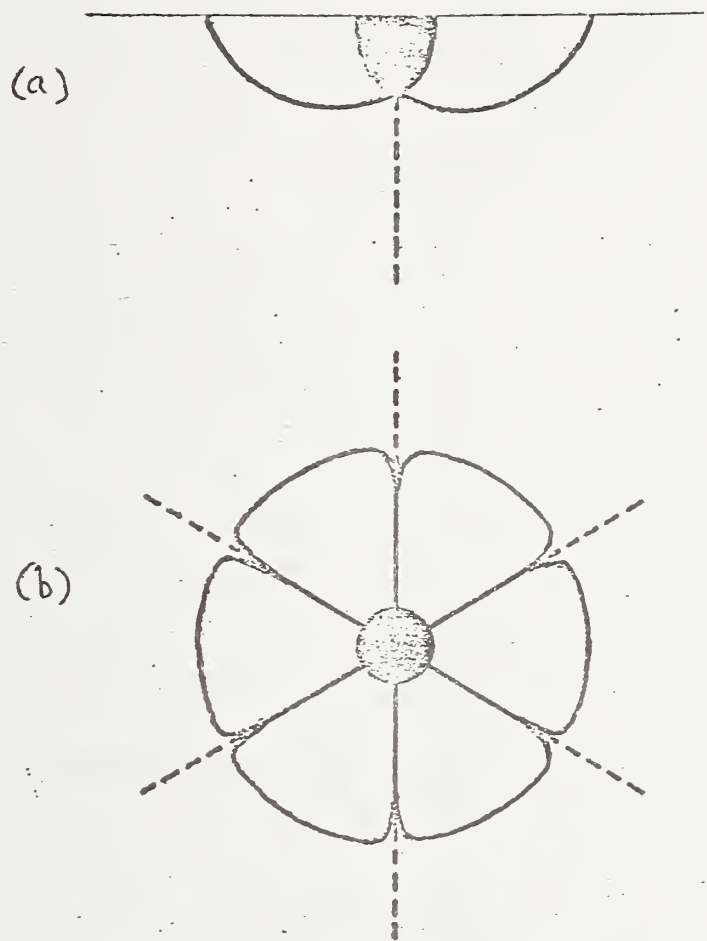
## References

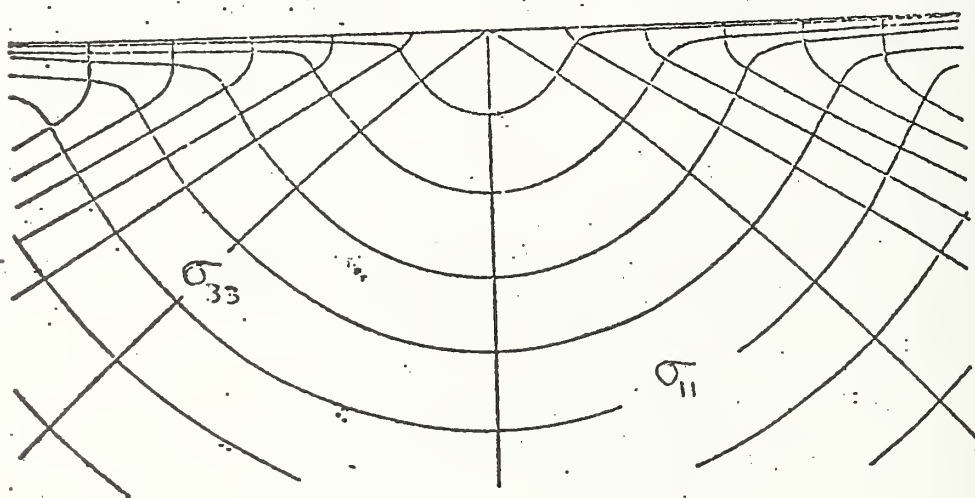
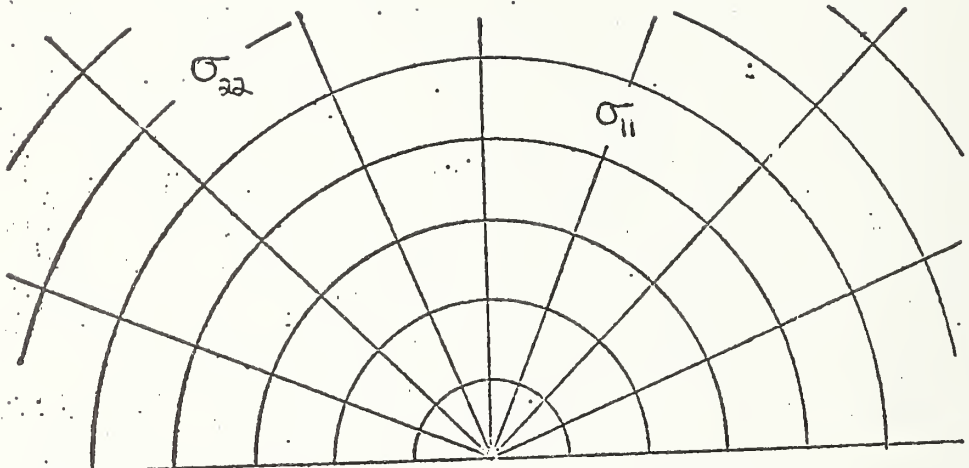
1. Lawn, B. R. and Wilshaw, T. R., J. Mater. Sci., in the press.
2. Lawn, B. R. and Swain, M. V., J. Mater. Sci., in the press.
3. Boussinesq, J., Application des Potentiels a l'Etude de l'Equilibre et du Mouvement des Solides Elastiques, (Gauthier-Villars, Paris, 1885). Discussed in Timoshenko, S. P. and Goodier, J. N., Theory of Elasticity (McGraw-Hill, New York, 1970), pp. 398-402.
4. Griffith, A. A., Phil. Trans. Roy. Soc. Lond., A211, 163 (1920).
5. Hertz, H., J. Reine Angew. Math., 92, 156 (1881); Verhandlungen des Vereins zur Beförderung des Gewerbe Fleisses, 61, 449 (1882). Reprinted in English, in Hertz's Miscellaneous Papers (Macmillian, London, 1896), Chs. 5, 6.
6. Frank, F. C. and Lawn, B. R., Proc. Roy. Soc. Lond., A299, 291 (1967).
7. Culf, C. J., J. Soc. Glass.Tech., 41, 157 (1957).
8. Hockey, B. J., in The Science of Hardness Testing and its Research Applications, Symposium Proceedings, Eds. Westbrook, J. H. and Conrad, H. (American Society for Metals, Metals Park, 1973), Ch. 3.
9. Wagatsume, R., Sumino, K., Uchida, W. and Yamamoto, S. J. Appl. Phys., 42, 222 (1971).
10. Kelly, A., Strong Solids (Clarendon, Oxford, 1966).
11. Hill, M. J. and Rowcliffe, D. J., J. Mater. Sci., in the press.
12. Ernsberger, F. M., Ann. Rev. Mat. Sci., 2, 529 (1972).
13. Mindlin, R. D., Physics, 7, 195 (1936).
14. Westbrook, J. H., in The Science of Hardness Testing and its Research Applications, Symposium Proceedings, Eds. Westbrook, J. H. and Conrad, H. (American Society for Metals, Metals Park, 1973), pp. 491-494.

15. Evans, A. G., J. Amer. Ceram. Soc., 56, 405 (1973).
16. Nadai, A., Theory of Flow and Fracture of Solids (McGraw-Hill, New York, 1963), pp. 247-249.
17. Carter, J. L. and MacGregor, I. D., Proc. Apollo 11 Lunar Sci. Conf., 1, 247 (1970).
18. Vedder, J. F. and Mandeville, J.-C., J. Geophys. Res., 79, 3247 (1974).

### Figure Captions

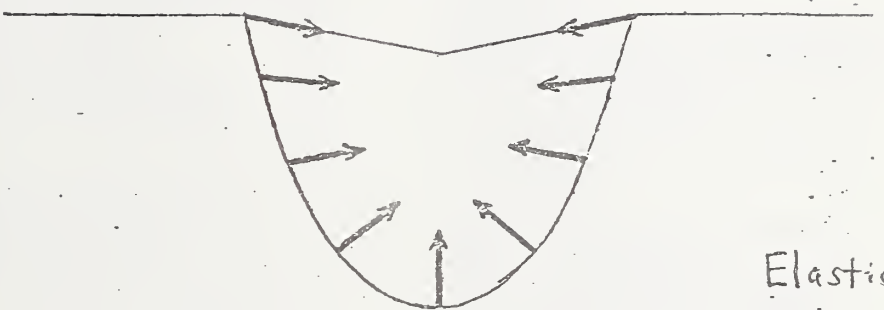
1. Fracture geometry beneath sharp indenter. Central deformation zone shown as dark region, median vent cracks as broken lines, lateral vent cracks as heavy lines. (a) Section view schematic, (b) plan view schematic, (c) surface view of fused silica indented with sharp, irregular particle (scanning electron micrograph).
2. Stress trajectories (curves whose tangent indicates direction of principal stress) for Boussinesq field, showing half-surface view (top) and section view (bottom). Cone cracks initiate from incipient surface flaws and propagate everywhere orthogonally to  $\sigma_{11}$  (tensile outside contact area), median vents initiate from central deformation zone and propagate orthogonally to  $\sigma_{22}$  (tensile below contact zone), lateral vents initiate from deformation zone and propagate nearly orthogonally to  $\sigma_{33}$  (compressive everywhere, but tensile if applied load reversed).
3. Schematic representation of distribution of mismatch tractions at boundary between central deformation zone and surrounding elastic matrix, at indenter withdrawal.





Deformation

zone



Elastic  
matrix



DISTRIBUTION LIST

Organization

Office of Naval Research  
Department of the Navy  
Attn: Code 471  
Arlington, Virginia 22217

Director  
Office of Naval Research  
Branch Office  
495 Summer Street  
Boston, Massachusetts 02210

Director  
Office of Naval Research  
New York Area Office  
207 West 24th Street  
New York, New York 10011

Director  
Office of Naval Research  
Branch Office  
1030 East Green Street  
Pasadena, California 91101

Commanding Officer  
Naval Weapons Laboratory  
Attn: Research Division  
Dahlgren, Virginia 22448

Director  
Naval Research Laboratory  
Attn: Technical Information Officer  
Code 2000  
Washington, D. C. 20390

Director  
Naval Research Laboratory  
Attn: Technical Information Officer  
Code 2020  
Washington, D. C. 20390

Director  
Naval Research Laboratory  
Attn: Technical Information Officer  
Code 6000  
Washington, D. C. 20390

Organization

Director  
Naval Research Laboratory  
Attn: Technical Information Officer  
Code 6100  
Washington, D. C. 20390

Director  
Naval Research Laboratory  
Attn: Technical Information Officer  
Code 6300  
Washington, D. C. 20390

Director  
Naval Research Laboratory  
Attn: Technical Information Officer  
Code 6400  
Washington, D. C. 20390

Director  
Naval Research Laboratory  
Attn: Library  
Code 2029 (ONRL)  
Washington, D. C. 20390

Commander  
Naval Air Systems Command  
Department of the Navy  
Attn: Code AIR 320A  
Washington, D. C. 20360

Commander  
Naval Air System Command  
Department of the Navy  
Attn: Code AIR 5203  
Washington, D. C. 20360

Commander  
Naval Ordnance Systems Command  
Department of the Navy  
Attn: Code ORD 033  
Washington, D. C. 20360

Commanding Officer  
Naval Air Development Center  
Aeronautical Materials Div.  
Johnsville  
Attn: Code MAM  
Warminster, Pa. 18974

Commanding Officer  
Naval Ordnance Laboratory  
Attn: Code 210  
White Oak  
Silver Spring, Maryland 20910

Commanding Officer  
Army Research Office, Durham  
Box CM, Duke Station  
Attn: Metallurgy & Ceramics Div.  
Durham, North Carolina 27706

Commander  
Naval Ship Systems Command  
Department of the Navy  
Attn: Code 0342  
Washington, D. C. 20360

Office of Scientific Research  
Department of the Air Force  
Attn: Solid State Div. (SRPS)  
Washington, D. C. 20333

Commanding Officer  
Naval Civil Engineering Laboratory  
Attn: Code L70  
Port Hueneme, California 93041

Defense Documentation Center  
Cameron Station  
Alexandria, Virginia 22314

Commander  
Naval Ship Engineering Center  
Department of the Navy  
Attn: Code 6101  
Washington, D. C. 20360

National Bureau of Standards  
Attn: Metallurgy Division  
Washington, D. C. 20234

Naval Ships R&D Laboratory  
Annapolis Division  
Attn: Code A800  
Annapolis, Maryland 21402

National Bureau of Standards  
Attn: Inorganic Materials Div.  
Washington, D. C. 20234

Commanding Officer  
Naval Ships R&D Center  
Attn: Code 747  
Washington, D. C. 20007

Atomic Energy Commission  
Attn: Metals & Materials Branch  
Washington, D. C. 20545

Commander Naval Weapons Center  
Naval Weapons Center  
Attn: Code 5560  
China Lake, California 93555

Argonne National Laboratory  
Metallurgy Division  
P. O. Box 299  
Lemont, Illinois 60439

Commander  
Naval Underseas Warfare Center  
Pasadena, California 92152

Brookhaven National Laboratory  
Technical Information Division  
Attn: Research Library  
Upton, Long Island, New York 11973

Scientific Advisor  
Commandant of the Marine Corps  
Attn: Code AX  
Washington, D. C. 20380

Library  
Bldg. 50, Room 134  
Lawrence Radiation Laboratory  
Berkeley, California 94720

Los Alamos Scientific Laboratory  
P. O. Box 1663  
Attn: Report Librarian  
Los Alamos, New Mexico 87544

Commanding Officer  
Army Materials and Mechanics  
Research Center  
Attn: Res. Programs Office (AMXMR-P)  
Watertown, Massachusetts 02172

Director  
Metals & Ceramics Division  
Oak Ridge National Laboratory  
P. O. Box X  
Oak Ridge, Tennessee 37830

Commanding Officer  
Naval Underwater Systems Center  
Newport, Rhode Island 02844

Aerospace Research Laboratories  
Wright-Patterson AFB  
Building 450  
Dayton, Ohio 45433

Defense Metals Information Center  
Battelle Memorial Institute  
505 King Avenue  
Columbus, Ohio 43201

Army Electronics Command  
Evans Signal Laboratory  
Solid State Devices Branch  
c/o Senior Navy Liaison Officer  
Fort Monmouth, New Jersey 07703

Commanding General  
Department of the Army  
Frankford Arsenal  
Attn: ORDBA-1320, 64-4  
Philadelphia, Pennsylvania 19137

Executive Director  
Materials Advisory Board  
National Academy of Sciences  
2101 Constitution Avenue, N. W.  
Washington, D. C. 20418

NASA Headquarters  
Attn: Code RRM  
Washington, D. C. 20546

Air Force Materials Lab  
Wright-Patterson AFB  
Attn: MAMC  
Dayton, Ohio 45433

Air Force Materials Lab  
Wright-Patterson AFB  
Attn: MAAM  
Dayton, Ohio 45433

Deep Submergence Systems Project  
Attn: DSSP-00111  
Washington, D. C. 20360

Advanced Research Projects Agency  
Attn: Director, Materials Science  
Washington, D. C. 20301

Department of the Interior  
Bureau of Mines  
Attn: Science & Engineering Advisor  
Washington, D. C. 20240

Defense Ceramics Information Center  
Battelle Memorial Institute  
505 King Avenue  
Columbus, Ohio 43201

National Aeronautics & Space Adm.  
Lewis Research Center  
Attn: Librarian  
21000 Brookpark Rd.  
Cleveland, Ohio 44135

Naval Missile Center  
Materials Consultant  
Code 3312-1  
Point Mugu, California 93041

Commanding Officer  
Naval Weapons Center Corona Labs.  
Corona, California 91720

Commander  
Naval Air Test Center  
Weapons Systems Test Div. (Code OLA)  
Patuxent River, Maryland 20670

Director  
Ordnance Research Laboratory  
P. O. Box 30  
State College, Pennsylvania 16801

Director  
Applied Physics Laboratory  
1013 Northeast Fortieth St.  
Seattle, Washington 98105

Materials Sciences Group  
Code S130.1  
271 Catalina Boulevard  
Navy Electronics Laboratory  
San Diego, California 92152

Dr. Waldo K. Lyon  
Director, Arctic Submarine Laboratory  
Code 90, Building 371  
Naval Undersea R&D Center  
San Diego, California 92132

Dr. R. Nathan Katz  
Ceramics Division  
U.S. Army Materials & Mechanics  
Research Center  
Watertown, Mass. 02172

SUPPLEMENTARY DISTRIBUTION LIST

Professor R. Roy .  
Materials Research Laboratory  
Pennsylvania State University  
University Park, Pennsylvania 16802

Professor D. H. Whitmore  
Department of Metallurgy  
Northwestern University  
Evanston, Illinois 60201

Professor J. A. Pask  
Department of Mineral Technology  
University of California  
Berkeley, California 94720

Professor D. Turnbull  
Div. of Engineering and Applied Sci.  
Harvard University  
Pierce Hall  
Cambridge, Massachusetts 02100

Dr. T. Vasilos  
AVCO Corporation  
Research and Advanced Development Div.  
201 Lowell St.  
Wilmington, Massachusetts 01887

Dr. H. A. Perry  
Naval Ordnance Laboratory  
Code 230  
Silver Spring, Maryland 20910

Dr. Paul Smith  
Crystals Branch, Code 6430  
Naval Research Laboratory  
Washington, D. C. 20390

Dr. A. R. C. Westwood  
RIAS Division  
Martin-Marietta Corporation  
1450 South Rolling Road  
Baltimore, Maryland 21227

Dr. W. Haller  
Chief, Inorganic Glass Section  
National Bureau of Standards  
Washington, D. C. 20234

Dr. R. H. Doremus  
General Electric Corporation  
Metallurgy and Ceramics Lab.  
Schenectady, New York 12301

Professor G. R. Miller  
Department of Ceramic Engineering  
University of Utah  
Salt Lake City, Utah 84112

Dr. T. D. Chikalla  
Fuels and Matls. Department  
Battelle Northwest  
P. O. Box 999  
Richland, Washington 99352

Mr. I . Berman  
Army Materials and Mechanics  
Research Center  
Watertown, Massachusetts 02171

Dr. F. F. Lange  
Westinghouse Electric Corporation  
Research Laboratories  
Pittsburgh, Pennsylvania 15235

Professor H. A. McKinstry  
Pennsylvania State University  
Materials Research Laboratory  
University Park, Pa. 16802

Professor T. A. Litovitz  
Physics Department  
Catholic University of America  
Washington, D. C. 20017

Dr. R. J. Stokes  
Honeywell Corporate Research Center  
10701 Lyndale Avenue South  
Bloomington, Minnesota 55420

Dr. Harold Liebowitz  
Dean of Engineering  
George Washington University  
Washington, D. C. 20006

Dr. H. Kirchner  
Ceramic Finishing Company  
P. O. Box 498  
State College, Pennsylvania 16801

Professor A. H. Heuer  
Case Western Reserve University  
University Circle  
Cleveland, Ohio 44106

Dr. D. E. Niesz  
Battelle Memorial Institute  
505 King Avenue  
Columbus, Ohio 43201

Dr. F. A. Kroger  
University of Southern California  
University Park  
Los Angeles, California 90007

Dr. Sheldon M. Wiederhorn  
National Bureau of Standards  
Inorganic Materials Division  
Washington, D. C. 20234

Dr. C. O. Hulse  
United Aircraft Research Labs  
United Aircraft Corporation  
East Hartford, Connecticut 06108

Professor M. H. Manghnani  
University of Hawaii  
Hawaii Institute of Geophysics  
2525 Correa Road  
Honolulu, Hawaii 96822

Dr. Stephen Malkin  
Department of Mechanical Engineering  
University of Texas  
Austin, Texas 78712

Prof. H. E. Wilhelm  
Department of Mechanical Engineering  
Colorado State University  
Fort Collins, Colorado 80521

Stanford University  
Dept. of Materials Sciences  
Stanford, California 94305

Dr. R. K. MacCrone  
Department of Materials Engineering  
Rensselaer Polytechnic Institute  
Troy, New York 12181

Dr. D. C. Mattis  
Belfer Graduate School of Science  
Yeshiva University  
New York, New York 10033

Professor R. B. Williamson  
College of Engineering  
University of California  
Berkeley, California 94720

Professor R. W. Gould  
Department of Metallurgical  
and Materials Engineering  
College of Engineering  
University of Florida  
Gainesville, Florida 32601

Professor V. S. Stubican  
Department of Materials Science  
Ceramic Science Section  
Pennsylvania State University  
University Park, Pennsylvania 16802

Dr. R. C. Anderson  
General Electric Company  
Miniature Lamp Department  
Nela Park  
Cleveland, Ohio 44112

Dr. Bert Zauderer  
MHD Program, Advanced Studies  
Room L-9513-VFSC  
General Electric Company  
P. O. Box 8555  
Philadelphia, Pennsylvania 19101

Prof. C. F. Fisher, Jr.  
Department of Mechanical and Aero-  
Space Engineering  
University of Tennessee  
Knoxville, Tennessee 37916

|  |  |  |  |                              |
|--|--|--|--|------------------------------|
| U.S. DEPT. OF COMM.<br>BIBLIOGRAPHIC DATA<br>SHEET   |  | 1. PUBLICATION OR REPORT NO.<br><br>NBSIR 75-659   | 2. Gov't Accession No.                                   | 3. Recipient's Accession No. |
| 4. TITLE AND SUBTITLE<br><br>A New Mode of Chipping Fracture in Brittle Solids, and Its Application in a Model for Wear Under Fixed Abrasive Conditions I. Mode of Chipping Fracture II. Wear Model"   |  | 5. Publication Date<br><br>February 1975   |  |                              |
| 7. AUTHOR(S)<br><br>Brian R. Lawn  |  | 6. Performing Organization Code  |  |                              |
| 9. PERFORMING ORGANIZATION NAME AND ADDRESS<br><br>NATIONAL BUREAU OF STANDARDS<br>DEPARTMENT OF COMMERCE<br>WASHINGTON, D.C. 20234  |  | 8. Performing Organ. Report No.<br><br>10. Project/Task/Work Unit No.<br>3130453                 |  |                              |
| 12. Sponsoring Organization Name and Complete Address (Street, City, State, ZIP)<br><br>Department of the Navy<br>Office of Naval Research<br>Arlington, Virginia 22217  |  | 11. Contract/Grant No.<br><br>13. Type of Report & Period<br>Covered Interim<br>7/1/74 - 6/30/75 |  |                              |
| 14. Sponsoring Agency Code<br>ONR  |  |  |  |                              |
| 15. SUPPLEMENTARY NOTES  |  |  |  |                              |
| 16. ABSTRACT (A 200-word or less factual summary of most significant information. If document includes a significant bibliography or literature survey, mention it here.)<br><br>A description is given of the mode of chipping fracture observed in highly brittle solids. It is pointed out that residual stresses about indentation deformation centers play a vital role. The implications of this mode in a number of mechanical phenomena are discussed. |  |  |  |                              |
| An explicit model for the wear of brittle surfaces under fixed abrasive conditions is presented in terms of indentation fracture concepts. The predicted wear rate for glass agrees with that observed experimentally to within an order of magnitude. Some implications concerning the parameters which influence the abrasion process, particularly the hardness, are discussed.   |  |  |  |                              |
| 17. KEY WORDS (six to twelve entries; alphabetical order; capitalize only the first letter of the first key word unless a proper name; separated by semicolons)<br><br>Abrasion; brittle solids; brittle surfaces; chipping; fracture; hardness; indentation; residual stress; stress analysis; wear rate  |  |  |  |                              |
| 18. AVAILABILITY<br><br><u>xxxx</u> For Official Distribution. Do Not Release to NTIS  |  | <input type="checkbox"/> Unlimited   | 19. SECURITY CLASS<br>(THIS REPORT)<br><br>UNCL ASSIFIED | 21. NO. OF PAGES<br><br>29   |
| <input type="checkbox"/> Order From Sup. of Doc., U.S. Government Printing Office<br>Washington, D.C. 20402, SD Cat. No. C13   |  | 20. SECURITY CLASS<br>(THIS PAGE)<br><br>UNCLASSIFIED  | 22. Price  |                              |
| <input type="checkbox"/> Order From National Technical Information Service (NTIS)<br>Springfield, Virginia 22151   |  |  |  |                              |

